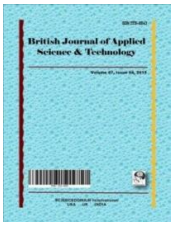

British Journal of Applied Science & Technology
9(2): 172-181, 2015, Article no.BJAST.2015.256
ISSN: 2231-0843

SCIENCEDOMAIN *international*
www.sciencedomain.org

The Focus on the Computation of Induced Magnetic Field in Magnetoplasmadynamic Thrusters

A. M. Tahsini[1*]

[1]*Aerospace Research Institute, Ministry of Science, Research and Technology, Tehran, Iran.*

Author's contribution

The sole author designed, analyzed and interpreted and prepared the manuscript.

Article Information

DOI: 10.9734/BJAST/2015/17531
Editor(s):
(1) Grzegorz Golański, Institute of Materials Engineering, Czestochowa University of Technology, Poland.
Reviewers:
(1) Anonymous, IIT Delhi, India.
(2) Philippe Reynier, Ingénierie et Systèmes Avancés, France.
(3) Swarniv Chandra, Physics Dept. Techno India University, Kolkata, India.
Complete Peer review History: http://www.sciencedomain.org/review-history.php?iid=1137&id=5&aid=9226

Original Research Article

Received 17th March 2015
Accepted 20th April 2015
Published 13th May 2015

ABSTRACT

Physical analysis of the magnetoplasmadynamic thrusters, especially ones with self induced magnetic field, demonstrates the interaction of applied electric and induced magnetic field to affect the flow field and accelerate it to reach the higher specific impulses. Such interaction besides changing the fluid state to the plasma, acts as momentum and energy source terms which should be predicted carefully. The former method which has been frequently used to compute the induced magnetic field is analyzed here and is shown that despite of its mathematical validity of the governing equation, it is disable to compute the induced magnetic field due to the problems in boundary condition. Therefore the accurate method is suggested here which shows much better abilities to study the induced magnetic field and can be utilized in performance analysis and numerical simulation of MPDTs.

Keywords: Induced magnetic field; magnetoplasmadynamic; numerical study; thruster.

NOMENCLATURE

A = *computational cell area*
$\vec{B}$ = *magnetic flux density vector*
$\vec{E}$ = *electric field intensity vector*
I = *electric current*
$\vec{J}$ = *electric current density vector*
$\vec{R}$ = *displacement vector*

**Corresponding author: E-mail: a_m_tahsini@yahoo.com;*

$\vec{u}$ = *velocity vector*
u = *axial component of velocity*
V = *electric potential*
v = *radial component of velocity*
x = *axial coordinate*
y = *radial coordinate*
μ = *magnetic permeability*
σ = *electric conductivity*
θ = *angular coordinate*

1. INTRODUCTION

Nearly all space propulsion requirements are satisfied by chemical propulsion systems, which are limited in performance by the stored energy within the propellants. One way to overcome this limitation is to increase a working gas exit velocity through additional energy supplied from external sources, like what happened in electric propulsion devices.

Basic electric propulsion systems use an electric power to transmit additional thermal energy to the flow field and increase the exhaust velocity. More advanced electric propulsion systems heat the propellant to an ionized state and then accelerate the produced plasma through electromagnetic forces. The low thrust generated by these magnetoplasmadynamic thrusters (MPDT) restricts their usage, but their simplicity of design and theoretical efficiency at high power levels make them ideal candidate as the primary propulsion sources for deep space missions such as satellite station-keeping and orbit rising. They can offer specific impulses that are orders of magnitude higher than chemical rockets.

The MPDT operates with applied or self-induced magnetic fields. In the self-induced configuration, the electric current ionizes the injected propellant through Joule heating and this current also induces a perpendicular (azimuthal) magnetic field which accelerates the plasma by the Lorentz force.

The ideas of electric propulsion devices go back to the 1920s, but first seriously studied in the 1950s and have 45 years operational history in different space programs. There are some experimental and numerical studies have been specifically done on self-field MPDTs, too. These studies can be categorized according to the assumed simplifying models, adopted numerical schemes, or based on technological viewpoints.

Some flow field assumptions are as: single fluid or multi fluid, isothermal or multi temperature, fully ionizes or partially ionized, viscous or free friction and with Hall Effect or not. Flow field analysis and simulation [1-18]; thrust, electric power and specific impulse estimation [19-27]; instability analysis [28-32]; geometry and propellant type effects [33-42] and electrode's erosion calculation [43-45] have been the main purpose of these studies. However it should be emphasized that this categorization is not very accurate and some overlaps exist.

In self-field MPDTs, the magnetic field is induced due to the applied electric field. Afterward, the interaction of this magnetic field and electric current play an important role on plasma acceleration due to the Lorentz force, as mentioned before. Therefore, an accurate calculation of the induced magnetic field in these thrusters is one of the basic foundations for precise simulation of MPDTs and their performance prediction. Although most studies in this area have been done numerically, some shortcomings can be found in magnetic field computation.

In the present study, after analysis of such shortcomings in common method, an accurate scheme to calculate the induced magnetic field is suggested. Using this procedure will be useful to improve the numerical simulation of self-field magnetoplasmadynamic thrusters.

2. GOVERNING EQUATIONS AND ANALYSIS

The complete set of governing equations for quasi steady, fully ionized, isothermal and single fluid flow field in MPDTs accompanies by the Navier-Stokes equations are the Maxwell's equations as presented here.

Faraday's law:

$$\nabla \times \vec{E} = 0 \tag{1}$$

Ohm's law:

$$\vec{J} = \sigma\left(\vec{E} + \vec{u} \times \vec{B}\right) \tag{2}$$

Ampere's law:

$$\nabla \times \vec{B} = \mu\vec{J} \tag{3}$$

And

$$\nabla.\vec{J} = 0 \tag{4}$$

Due to the Ohm's law which contains the velocity vector term, the flow field and electromagnetic governing equations are coupled. Moreover, the electromagnetic field affects substantially the flow field due to the applied momentum and energy sources:

Lorentz force (momentum source):

$$\vec{J} \times \vec{B} \tag{5}$$

Joule heating (energy source):

$$\vec{J}.\vec{E} \tag{6}$$

Therefore the set of all equations should be solved to find the electric field, magnetic field, electric current and flow field properties such as velocity vector and temperature. The magnetic field appears in the both Ohm's law and Lorentz force and affects the electric current density as well as fluid acceleration. Additionally, it is induced due to the electric current in conducting media (plasma). The question is how to calculate this magnetic field.

Nearly all studies have been already done use the similar procedure which is presented here. In an axisymmetric thruster, only angular magnetic field exists. In addition, the electric field and electric current just has radial and axial components. So the Maxwell's equations are:

$$\frac{\partial E_y}{\partial x} - \frac{\partial E_x}{\partial y} = 0 \tag{7}$$

$$J_x = \sigma(E_x + vB_\theta) \tag{8}$$

$$J_y = \sigma\left(E_y - uB_\theta\right) \tag{9}$$

$$\frac{\partial B_\theta}{\partial y} + \frac{B_\theta}{y} = \mu J_x \tag{10}$$

$$-\frac{\partial B_\theta}{\partial x} = \mu J_y \tag{11}$$

Combining these equations and omitting the electric field as well as electric current yields the below equation which shows the balance between convection and diffusion of angular component of magnetic field.

$$\left[\frac{\partial(uB_\theta)}{\partial x} + \frac{\partial(vB_\theta)}{\partial y}\right] - \left(\frac{1}{\mu\sigma}\right)\left[\frac{\partial^2 B_\theta}{\partial x^2} + \frac{\partial^2 B_\theta}{\partial y^2} + \frac{1}{y}\frac{\partial B_\theta}{\partial y} - \frac{B_\theta}{y^2}\right] = 0 \tag{12}$$

This equation is quite true from mathematical viewpoint, but from physical viewpoint, it works well if appropriate boundary conditions are applied. This is exactly the origin of the imperfection of previous studies. They have used the boundary condition at inlet of thruster as below, without reasonable explanation [for example 12,13,16].

$$B_\theta = \frac{\mu I}{2\pi y} \tag{13}$$

This seems to be a common mistake. It is helpful to check the origin of this equation. They have only referred it to the Ampere's law. It is like a magnetic field distribution around a current-carrying wire.

Using the Ampere's law for axisymmetric geometry (equations 10,11) and assuming just axial electric current results to the remaining equation:

$$\frac{1}{y}\frac{\partial(yB_\theta)}{\partial y} = \mu J_x \tag{14}$$

Therefore, it can be integrated as:

$$B_\theta = \frac{\mu}{y}\int_0^R J_x y dy \tag{15}$$

Then, assuming a constant axial electric current density, it yields:

$$B_\theta = \frac{\mu J_x R^2}{2y} \tag{16}$$

Which is as exactly the same as equation 13 considering $J_x = I/(\pi R^2)$ here. The assumptions which are used to derive this relation aren't applicable in MPDTs, because there is indeed radial and variable electric current density (see Fig. 1) instead of assumed axial and constant electric current density which is used to derive eq. (16). Therefore, using eq. (13) as a boundary condition for equation 12 yields a wrong distribution of induced magnetic flux density.

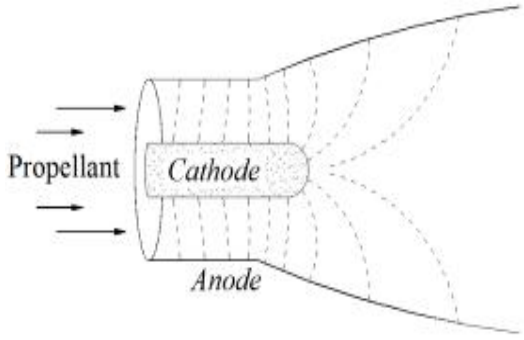

Fig. 1. Electric current lines in typical MPDT

In addition, using equation 12 with applying eq. (13) as a boundary condition instead of applying correct B. C. only yields a variation of induced magnetic field without any change in sign despite the fact that a change in magnetic field direction must be observed in these geometries, which will be shown later (in Fig. 5). This phenomenon, however, has not been considered before.

To overcome such problems and compute accurately the induced magnetic flux density, direct solution of the Ampere's law (eq. 3) is suggested. The solution is as follows which should be calculated numerically.

$$\vec{B} = \frac{\mu}{4\pi} \iiint_{\forall} \frac{\vec{J} \cdot \vec{R}}{R^3} d\forall \tag{17}$$

At first, Due to the steady Faraday's law, one can define the electric potential V where:

$$\vec{E} = -\nabla V \tag{18}$$

Combining equations 2, 4 and 18 yields the Poisson's equation for electric potential as:

$$\nabla^2 V = \nabla . \left(\vec{u} \times \vec{B} \right) \tag{19}$$

Therefore applying the potential level of cathode and anode (which is the input of problem) as a boundary condition of equation 19 determines directly the electric potential distribution and next the electric field from equation 18. Then, using equation 2 specifies the electric current. Finally, equation 17 can be solved to find the induced magnetic field.

It should be emphasized that in the simulation of axisymmetric fields, the two-dimensional grids are used but equation 17 is a three-dimensional integral. Thus the imaginary data on angular sections of the flow field must be generated and used as explained in next part.

3. NUMERICAL PROCEDURE AND RESULTS

The finite volume method is used here to discretize the Poisson's equation 19 to find the electric potential distribution. Although the Maxwell's equations should be solved simultaneously with the flowfield equations, but the focus is only on electromagnetic field's computation in the present study. Thus, there is no simulation and discussion on flow. The author has enough experiences on numerical computation of the flow field [46-49].

The ghost cells are used to apply the boundary conditions. The specified electric potential are applied on electrodes and the normal change of electric potential is zero on insulators. The electric current and displacement vectors in three dimensions are defined as below, where subscripts 1 shows all cells and subscripts 2 shows the specific cell in which magnetic field should be computed.

$$\vec{J} = J_x \hat{x} + J_y \hat{y} + J_z \hat{z} \tag{20}$$

$$\vec{R} = (x_2 - x_1)\hat{x} + (y_2 - y_1)\hat{y} + (z_2 - z_1)\hat{z} \tag{21}$$

Computing the cross product in equation 17 and considering:

$$y = r \cos\theta \tag{22}$$

$$z = r \sin\theta \tag{23}$$

And regarding that the electric current in imaginary angular plates is simple function of the referenced plate as:

$$J_x = J_{x_{\theta=0}} \tag{24}$$

$$J_y = J_{y_{\theta=0}} \cos\theta \tag{25}$$

One can find the magnetic field at point 2 as:

$$B_\theta = \frac{\mu}{4\pi}\iiint_{\forall} \frac{J_{x_{\theta=0}}(y_2 - y_1\cos\theta) - J_{y_{\theta=0}}\cos\theta\,(x_2 - x_1)}{[(x_2 - x_1)^2 + (y_2)^2 + (y_1)^2 - 2y_2y_1\cos\theta]^{3/2}}\,d\forall \tag{26}$$

It is replaced by the next summation in numerical procedure according to $d\forall = \left(\frac{2\pi}{k_{max}}\right) y_1 A_1$.

$$B_\theta(m,n) = \frac{\mu}{4\pi}\left(\frac{2\pi}{k_{max}}\right)\sum_{i=1}^{i_{max}}\sum_{j=1}^{j_{max}}\sum_{k=1}^{k_{max}}\left(\frac{F-G}{H}\right)y(i,j)A(i,j) \tag{27}$$

Where

$$F = J_x(i,j)\left(y(m,n) - y(i,j)\cos\left(\frac{2\pi(k-1)}{k_{max}}\right)\right) \tag{28}$$

And

$$G = J_y(i,j)\cos\left(\frac{2\pi(k-1)}{k_{max}}\right)\big(x(m,n) - x(i,j)\big) \tag{29}$$

And

$$H = \left[\big(x(m,n) - x(i,j)\big)^2 + \big(y(m,n)\big)^2 + \big(y(i,j)\big)^2 - 2y(m,n)y(i,j)\cos\left(\frac{2\pi(k-1)}{k_{max}}\right)\right]^{3/2} \tag{30}$$

The electromagnetic field is accurately calculated using this procedure iteratively until the solution is converged. One can use equation 26 with some algebraic efforts and shows that it yields exactly the magnetic field distribution around and within the current-carrying wire which is found in text books. So the suggested procedure can be used numerically to study the complicated problems as MPDTs instead of questionable previous common method.

Here, the magnetic field between two concentric electrodes in quiescent flow is considered. The cathode and anode are corresponding parts on two cylinders as shown in Fig. 2.

The electric potential difference of 1 KV is applied to the electrodes with inner and outer radius of 0.02 m and 0.1 m respectively. The cylinder length is 0.3 m which it's one third is electrode. The electric conductivity is assumed 20 A/Vm. The electric potential contours are presented in Fig. 3. Each line shows 100 V difference. Due to the axial symmetry, the mean potential level is closer to the cathode; it is different from two-dimensional distribution. The electric current lines are shown in Fig. 4. The contours of angular magnetic flux density are presented in Fig. 5. It shows that the magnetic field magnitude has symmetry with respect to the vertical plate of symmetry but with opposite sign. The magnetic field is anticlockwise at the left of domain and is clockwise at right. The magnetic field distribution on the outer cylinder is shown in Fig. 6 using different grids which show the grid-independency of results.

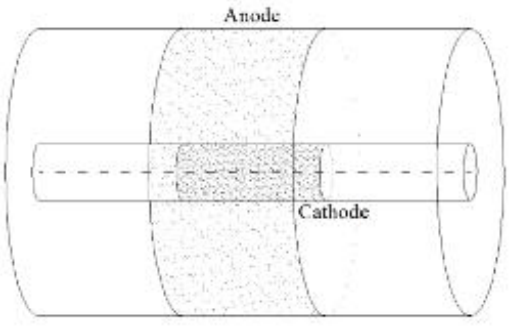

Fig. 2. Concentric electrodes

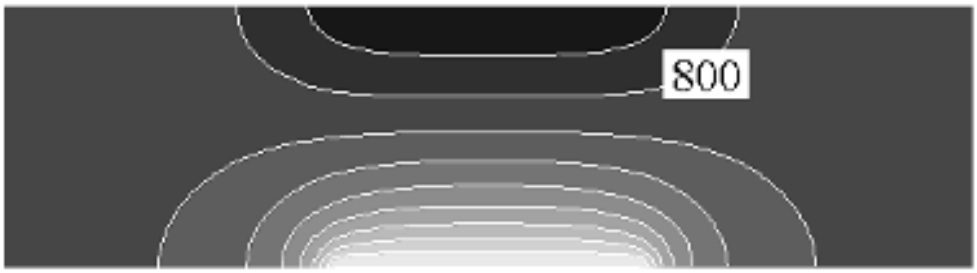

Fig. 3. Equipotential lines between concentric electrodes

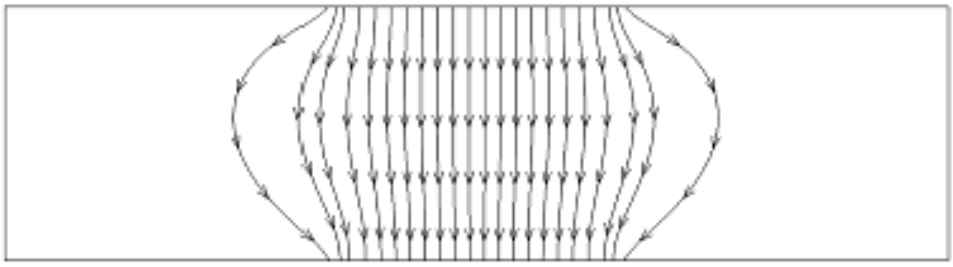

Fig. 4. Electric current lines between concentric electrodes

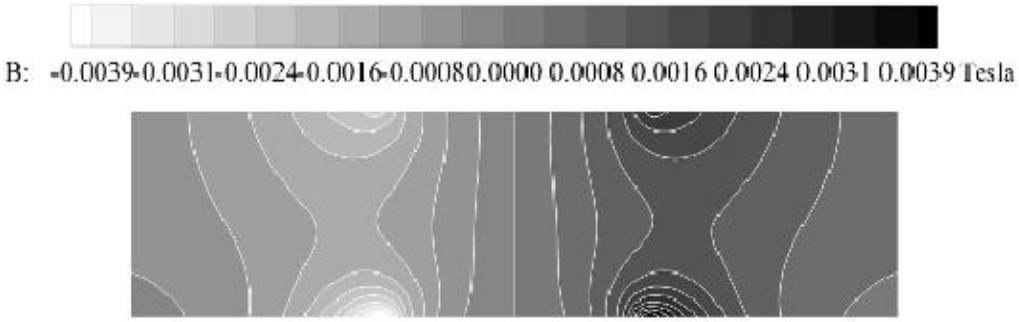

Fig. 5. Contours of angular magnetic flux density between concentric electrodes

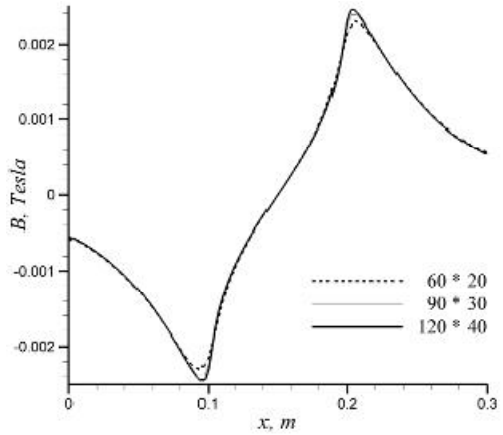

Fig. 6. Magnetic field distribution on the outer cylinder

Finally, this computation is repeated for the axisymmetric nozzle geometry (as Fig. 7). The electric potential difference and conductivity are 1 KV and 20 A/Vm respectively. Equipotential and electric current lines are presented in Fig. 8. The contours of angular magnetic flux density in this geometry are presented in Fig. 9. Here, the induced magnetic field's range is from -4.6 mT to +1 mT and is computed equal to zero on axis of symmetry as expected.

The magnetic field profile at the inlet is shown in Fig. 10. It shows that the magnetic field is not inversely proportional to the radial position as eq. 13. The total electric current is calculated here about 1.2 kA, so using eq. 13 shows the maximum magnetic field of 11 mT. On the other hand, the accurate computation shows the

magnitude of 1.3 mT (Fig. 10). Therefore, the vital discrepancy is observed between these two results that confirms the importance of using accurate method of induced magnetic field's computation in comparison with inappropriate method which has been used frequently. Such a mistake yields the errors on estimating the Lorentz force and electric current in relevant problems.

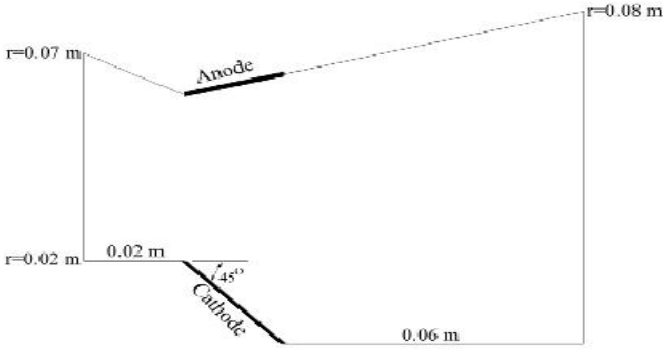

Fig. 7. Nozzle geometry

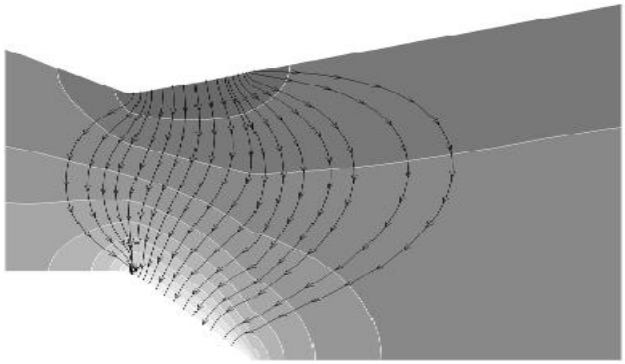

Fig. 8. Electric current and equipotential lines in nozzle

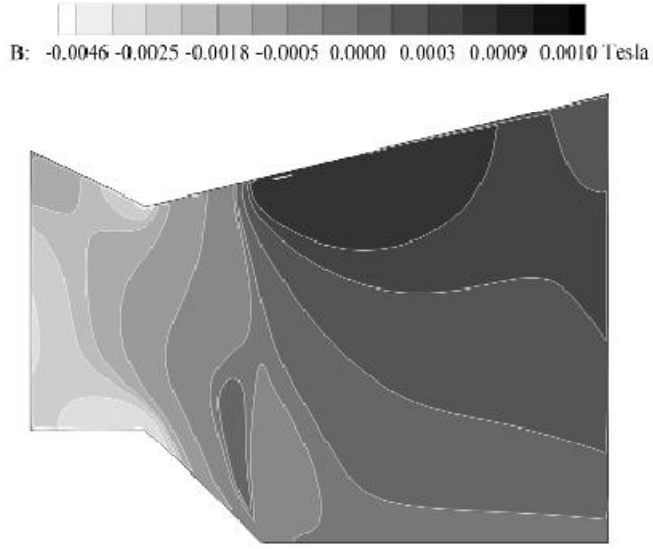

Fig. 9. Contours of angular magnetic flux density in nozzle

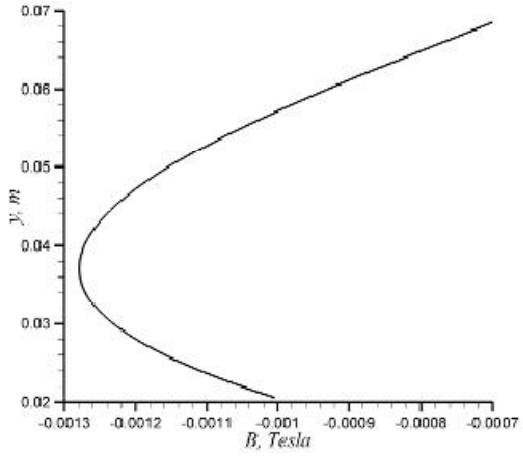

Fig. 10. Magnetic field profile at the nozzle inlet

4. CONCLUSION

In the present study, the accurate method to compute the induced magnetic field is suggested to be utilized to study numerically the magnetoplasmadynamic thrusters or similar problems. This method is direct solution of the Ampere's law, which yields a three-dimensional integration that should be computed numerically. The former method is analyzed and is shown that is not accurate due to the lack of proper boundary conditions. Typical problem is investigated to show the disability of common method in predicting the induced magnetic field variation and direction, which is vital to study carefully the performance of MPDTs. Using the suggested method leads to accurate distribution of the induced magnetic fields.

COMPETING INTERESTS

Author has declared that no competing interests exist.

REFERENCES

1. Mikellides PG. Modeling and analysis of a megawatt-class magnetoplasmadynamic thruster. Journal of Propulsion and Power. 2004;20(2):204-210.
2. Chanty JMG, Martinez-Sanchez M. Two-dimensional numerical simulation of MPD flows. AIAA 19th International Electric Propulsion Conference, 11-13 May 1987, Colorado, AIAA-87-1090; 1987.
3. Sleziona PC, Auweter-Kurtz M, Schrade HO. Numerical codes for cylindrical MPD thrusters. 20th International electric propulsion conference, 3-6 October 1988, Germany, IEPC-88-038; 1988.
4. Auweter-Kurtz M, Kurtz HL, Schrade HO, Sleziona PC. Numerical modelinf of the flow discharge in MPD thrusters. Journal of Propulsion and Power. 1989;5(1):49-55.
5. Sleziona PC, Auweter-Kurtz M, Schrade, HO. Numerical evaluation of MPD thrusters. AIAA 21st International Electric Propulsion Conference. 18-20 July 1990, Orlando, AIAA-90-2602; 1990.
6. Sleziona PC, Auweter-Kurtz M, Schrade H. O. MPD thrusters calculation considering high ionization modes. 22nd International Electric Propulsion Conference, 14-17 October 1991, Italy, IEPC-91-087; 1991.
7. Lapointe MR. Numerical simulation of self-field MPD thrusters. AIAA 27th Joint Propulsion Conference, 24-27 June 1991, Sacramento, AIAA-91-2341; 1991.
8. Caldo G, Choueiri EY, Kelly AJ, Jahn RG. Numerical simulation of MPD thruster flows with anomalous transport. AIAA 28th Joint Propulsion Conference, 6-8 July 1992, Sacramento, AIAA-92-3738; 1992.
9. Tilley DL, Castillo S. A comparison of theory and measurements in the anode region of a self-field MPD thruster. AIAA 30th Joint Propulsion Conference, 27-29 June 1994, Indianapolis, AIAA-94-3337; 1994.
10. Miyasaka T, Fujiwara T. An efficient numerical analysis of fully ionized plasma flows in a self-field MPD thruster. 24th International Electric Propulsion Conference, 19-23 September 1995, Moscow, IEPC-95-169; 1995.
11. Winter MW, Auweter-Kurtz M, Kurtz HL, Schrade HO. Evaluation of cathode temperature distribution in a cylindrical MPD thruster. 24th International Electric Propulsion Conference, 19-23 September 1995, Moscow, IEPC-95-109; 1995.
12. Sleziona PC, Auweter-Kurtz M. Numerical calculation of MPD thrusters. AIAA 31st Joint Propulsion Conference, 10-13 July 1995, San Diego, AIAA-95-2679; 1995.
13. Sankaran K, Choueiri EY, Jardin SC. Application of a new numerical solver to the simulation of MPD flows. AIAA 36th Joint Propulsion Conference, 16-19 July 2000, Alabama, AIAA-2000-3537; 2000.
14. Heierman J, Auweter-Kurtz M. Numerical and experimental investigation of the current distribution in self-field magnetoplasmadynamic thrusters. Journal

of Propulsion and Power. 2005;21(1):119-128.
15. Heierman J, Auweter-Kurtz M. Numerical investigation of the electrodes in high power self-field MPD thrusters. AIAA 33rd Plasmadynamics and Lasers Conference, 20-23 May 2002, Hawaii, AIAA-02-2102; 2002.
16. Sankaran K, Choueiri EY, Jardin SC. Comparison of simulated magnetoplasma-dynamic thruster flowfields to experimental measurements. Journal of Propulsion and Power. 2005;21(1):129-138.
17. Kubota K, Funaki I, Okuno Y. Numerical sturdy on electrode model for plasma simulation of MPD thruster. 32nd International Electric Propulsion Conference, 11-15 September 2011, Germany, IEPC-2011-252; 2011.
18. Kubota K, Funaki I, Okuno Y. Numerical study of plasma behavior in a magnetoplasmadynamic thruster around critical current. Journal of Propulsion and power. 2009;25(2):397-405.
19. Sleziona PC, Auweter-Kurtz M, Schrade HO, Wegmann T. Comparison of numerical and experimental investigations of nozzle type MPD accelerators. AIAA 21st International Electric Propulsion Conference, 18-20 July 1990, Orlando, AIAA-90-2663; 1990.
20. Gallimore AD, Kelly AJ, Jahn RG. Anode power deposition in magnetoplasmadynamic thrusters. Journal of Propulsion and power. 1993;9(3):361-368.
21. Sleziona PC, Auweter-Kurtz M, Schrade, HO. Numerical calculation of a cylindrical MPD thruster. 23rd International Electric Propulsion Conference, 13-16 September 1993, Seattle, IEPC-93-066; 1993.
22. Caldo G, Choueiri EY, Kelly AJ, Jahn RG. Numerical fluid simulation of a MPD thruster with real geometry. 23rd International Electric Propulsion Conference, 13-16 September 1993, Seattle, IEPC-93-072; 1993.
23. Mikellides PG. Design and operation of MW-class MPD thrusters Part I: Numerical modeling. 27th International Electric Propulsion Conference, 14-19 October 2001, California, IEPC-01-124; 2001.
24. Berry KJ, Roy S. Least square FE based MPD algorithm for practical magneto-plasma applications. AIAA 39th Aerospace Science Meeting and Exhibit, 8-11 January 2001, Reno, AIAA-01-0200; 2001.
25. Kubota K, Funaki I, Okuno Y. Numerical investigation of ionization and acceleration processed in a self-field MPD thruster. 29th International Electric Propulsion Conference, 1-4 November 2005, Princeton Univ. IEPC-2005-089; 2005.
26. Heimerdinger DJ, Martinez-Sanchez M. Fluid mechanics in a magnetoplasma-dynamic Thrusters. 20th International Electric Propulsion Conference, 3-6 October 1988, Germany, IEPC-88-039; 1988.
27. Niewood EH, Martinez-Sanchez M. The hall effect in a numerical model of MPD thrusters. 22nd International Electric Propulsion Conference, 14-17 October 1991, Italy, IEPC-91-099; 1991.
28. Wagner HP, Kaeppeler HJ, Auweter-Kurtz M. Instabilities in MPD thruster flows: Investigation of drift and gradient driven instabilities using multi-fluid plasma models. Journal of Physics D: Applied Physics. 1998;31:529-541.
29. Miyasaka T, Fujiwara T. Numerical study of onset phenomena in a 2-dimensonal axisymmetric MPD thruster. 26th International Electric Propulsion Conference, 17-21 October 1999, Japan, IEPC-99-168; 1999.
30. Uribarri L, Choueiri EY. Creation of onset voltage hash by Anode Spots in a magnetoplasmadynamic thruster. Journal of Propulsion and Power. 2009;25(4):949-957.
31. Tilley DL, Choueiri EY, Kelly AJ, Jahn RG. Microinstabilities in a 10-kilowatt self-field magnetoplasmadynamic thruster. Journal of Propulsion and Power. 1996;12(2):381-389.
32. Subramaniam VV, Lawless JL. Onset in magnetoplasmadynamic thrusters with finite-rate lionization. Journal of Propulsion and Power. 1988;4(6):526-532.
33. Sleziona PC, Auweter-Kurtz M, Schrade HO. Numerical calculation of nozzle type and cylindrical MPD thrusters. AIAA 28th International Electric Propulsion Conference, 6-8 July 1992, Orlando, AIAA-92-3296; 1992.
34. Lapointe MR. Numerical simulation of geometric scale effects in cylindrical self-field MPD thrusters. AIAA 28th Joint Propulsion Conference, 6-8 July 1992, Sacramento, AIAA-92-3297; 1992.
35. Lapointe MR. Numerical Simulation of cylindrical self-field MPD thrusters with multiple propellants. NASA Lewis

Research Center, NASA-C-R-194458; 1994.

36. Choueiri E. Scaling of thrust in self-field magnetoplasmadynamic thrusters. Journal of Propulsion and Power. 1998;14(5):744-753.
37. Nakata D, Toki K, Funaki I, Shimizu Y, Kuninaka H, Arakawa Y. Experimental verification of the nozzle shape optimization for self-field MPD thruster. 29th International Electric Propulsion Conference, 1-4 November 2005, Princeton Univ. IEPC-2005-163; 2005.
38. Kubota K, Funaki I, Okuno Y. Numerical sturdy of electrode geometry effects on flowfield in two-dimensional MPD Thrusters. 30th International Electric Propulsion Conference, 17-20 September 2007, Italy, IEPC-2007-87; 2007.
39. Takahashi Y, Ohtake R, Nakane N, Ishikawa Y, Kubota K, Funaki I. Optimum design guidelines on MPD thrusters around critical current. 32nd International Electric Propulsion Conference, 11-15 September 2011, Germany, IEPC-2011-033; 2011.
40. Mahendhran M, Kumar A. Numerical sturdy on the effect of electrode geometry in MPD thrusters. 32nd International Electric Propulsion Conference, 11-15 September 2011, Germany, IEPC-2011-228; 2011.
41. Sato H, Kubota K, Funaki I. Modeling and numerical simulation of a two-dimensional MPD thruster using a hydrogen propellant. 32nd International Electric Propulsion Conference, 11-15 September 2011, Germany, IEPC-2011-258; 2011.
42. Colasurdo G, Casalino L. Optimal Geometry of self-field magnetoplasma-dynamic thrusters. Journal of Propulsion and Power. 2001;17(2):472-474.
43. Polk JE, Kelly AJ, Jahn RG. Characterization of cold cathode erosion processes. 20th International Electric Propulsion Conference, 3-6 October 1988, Germany, IEPC-88-075; 1988.
44. Schrade HO, Auweter-Kurtz M, Kurtz HL. Cathode erosion studies on MPD thrusters. AIAA Journal. 1987;25(8):1105-1112.
45. Myers RM, Suzuki N, Kelly AJ, Jahn RJ. Cathode Phenomena in a low power magnetoplasmadynamic thruster. Journal of Propulsion and Power. 1991;7(5):760-766.
46. Tahsini AM. Heat Release effects on drag reduction in high speed flows. International Journal of Heat and Mass Transfer. 2013;57(2):657-661.
47. Tahsini AM. Ignition Delay time in swirling supersonic flow. ACTA Astronautica. 2013;83:91-96.
48. Tahsini AM. Piloted ignition of solid fuels in turbulent back-step flows. Aerospace Science and Technology. 2012;18(1):8-14.
49. Tahsini AM. Turbulence and additive effects on ignition delay in supersonic combustion. *IMech E.* Journal of Aerospace Engineering. 2013;227(1):93-99.

Peer-review history:
The peer review history for this paper can be accessed here:
http://www.sciencedomain.org/review-history.php?iid=1137&id=5&aid=9226